Water Supply

IWA PUBLISHING

Water Supply Vol 24 No 3, 835 doi: 10.2166/ws.2024.027

Time-averaged flow characterisations in a bimodal gravel-bed stream and relative role of sediment depositions on near-bed coherent flow structures

Ratul Das[a,*], Pritam Malakar[b] and Akash Datta[a]

[a] Department of Civil Engineering, National Institute of Technology Agartala, Tripura, 799046, India
[b] Civil Engineering Department, G. H. Raisoni University Amravati, Maharashtra 444701, India
*Corresponding author. E-mail: ratulnitagartala@gmail.com

ABSTRACT

The present study aims to quantify experimentally the relative role of sediment depositions on near-bed flows and turbulence in a gravel-bed stream. Time-averaged velocity was measured over a sand-filled gravel-bed stream with four cases of sediment depositions and compared with those over a gravel-bed stream without sediment depositions. An acoustic Doppler velocimeter was used to measure the instantaneous velocity of flows. The progressive infilling of void spaces in the gravel-bed stream forms distinct bimodal depositions that alter the mean flows characterised by increasing zero-velocity levels and massive damping in the bed shear stresses. The data plots of turbulent intensity depict enhancement of streamwise turbulent intensity in the near-bed flow region with increasing sand depositions. Moreover, the opposite nature of streamwise and vertical turbulent kinetic energy fluxes in the interfacial sublayer leads to slowing down the time-average Reynolds shear stresses at the vicinity of the gravel-bed surface. At the vicinity of the crest, the ejection and sweep events contributed approximately 86 and 56%, respectively, to the total Reynolds shear stress production in the case of gravel bed under clear-water flow conditions. By contrast, the contributions of turbulent sweep events increased over the sand-filled gravel bed at the same location.

Key words: gravel bed, interfacial sublayer, Reynolds shear stress, sand-filled gravel bed, sweep events, turbulence

HIGHLIGHTS

- Sediment particle entrainment and interstices within the pore spaces of a gravel bed.
- Results are compared with the flows over an immobile gravel-bed stream under clear-water flow conditions.
- A higher level of sand deposition depicts massive damping in the near-bed Reynolds shear stress profiles.

INTRODUCTION

Mean flows and turbulence over bimodal rough beds have received much attention in recent years. In fact, most of the available field and experimental investigations in this regard have been carried out either on unimodal smooth or rough bed streams. These investigations are adequate to broaden the knowledge, but the sediment entrainment, deposition, and transport on the gravel bed and the bimodal nature have a vital role on the near-wall turbulent flow characteristics in rivers and streams. There has been relatively limited research carried out considering the bimodal nature of such a stream bed (Ferguson *et al.* 1989; Sambrook-Smith & Ferguson 1995, 1996). Some researchers have addressed the role of sand coverage in rough bed streams on bed-load transport rate and demonstrated the possible morphodynamical changes (Wilcock & Kenworthy 2002; Almedeij & Diplas 2003; Best 2005). In recent years, the problem of morphodynamical changes in rough bimodal beds has been dealt with for sediment entrainment, depositions, and other factors concerned with the transport of finer bed particles (Dey & Raikar 2007; Grams & Wilcock 2007; Gaudio *et al.* 2011). Moreover, it is also reported that the finer sediment in the gravel bed influences the processes of sediment entrainment and transport (Iseya & Ikeda 1987; Dietrich & Whiting 1989; Ferguson *et al.* 1989; Wilcock 1993; Sambrook-Smith & Ferguson 1996). During sediment entrainment, deposition, and transport, the finer particles are accelerated by the flows and decelerated by gravel-bed resistance. Hence, a large portion of particle momentum is transferred into the bed and dissipated, while only a small portion of it can be recovered by the flows. Consequently, the sediment depositions and alteration in bed roughness play a key role in the mean flow distribution (Grams & Wilcock 2007). Researchers also reported higher velocity gradients and enhanced

near-wall velocity distributions (Robert *et al.* 1992; Sambrook-Smith & Nicholas 2005). In a laboratory experimental study, Robert *et al.* (1992) showed that the alteration in the bed roughness resulted in higher velocity gradients and shear stresses in the near-wall flow region. It is also reported that the patches of finer sediment on a gravel bed impact the velocity distributions and bed shear stress (Ferguson *et al.* 1989; Robert *et al.* 1992). Sambrook-Smith & Nicholas (2005) investigated the flow turbulence on variable bed roughness and found enhanced near-wall velocity distributions with damping in shear stress distributions. It is shown that the gradual infilling of the gravel bed results in lesser bed shear stresses and imposes higher turbulence intensity and sweep-dominated turbulence in the near-bed flow region (Grams & Wilcock 2007; Wren *et al.* 2011). The thickness of finer sediment depositions relative to large roughness elements is the controlling factor to alter the near-wall flow characteristics. The results of a recent experimental study on turbulent flow characteristics over a sand–gravel mixed bed revealed a decrease of time-averaged longitudinal velocity in the near-wall flow region and reduction of the von Kármán coefficient from the universal value (Sharma 2021). A field study on a bimodal sediment bed composed of quartz sand base overlaying with gravel conducted by Thorne *et al.* (1989) showed that the sweeps and outward interactions dominate the Reynolds shear stress (RSS) and reported them to be the principal controlling factors in initiating and transporting coarse sediments. Conversely, ejection and inward interaction do not play any important roles in sediment transport. In fact, the coherent flow structures lead to corroborate the role of different turbulent burst events as the sweep events are associated with the inrush of high-speed fluid streaks towards the bed and significant in a bimodal stream bed. Moreover, the need for coherent structures is addressed by many researches to explore the fluid–sediment particle interactions (Williams *et al.* 2003; Cellino & Lemmin 2004; Yuan *et al.* 2009; Shih *et al.* 2017). In many studies, it was also observed that the roughness elements, size, shape, and orientations of bed particles can also significantly alter the local flow fields and large-scale coherent flow structures (Bathurst 1987; Dey *et al.* 2011; Dey & Das 2012). Bed-load transport and associated bursting phenomenon was examined in several studies and the finer sediment during bed-load transport interacts with coherent wall structures developing hair pin vortices that detach from the wall and enhancing the turbulent sweep events (Drake *et al.* 1988; Gyr & Schmid 1997). Moreover, the results of some experimental studies revealed that the bed-load transport is controlled by both sweep events with high-speed fluid and outward interaction events owing to strong streamwise velocity (Heathershaw & Thorne 1985; Cellino & Lemmin 2004; Wallace 2016). Therefore, the present study aims to quantify the near-bed turbulence in a sand-filled gravel-bed stream and to compare it with that under clear-water flow conditions. Also, the study aims to address the nature of time-averaged streamwise and vertical turbulent kinetic energy (TKE) fluxes to corroborate the damping of bed shear stresses in sand-filled gravel-bed streams.

EXPERIMENTATION

Laboratory experiments were carried out in a rectangular flume that was 15 m long, 0.91 m wide, and 0.80 m deep. The flume bed was made with five layers of uniform gravels ($d_{50} = 0.04$ m) as shown in Figure 1(a). At the commencement of an experimental run, the gravel bed was manually screeded and levelled. A longitudinal bed slope of 0.25% was maintained throughout the length of the flume. A sediment hopper was used at the upstream end of the flume to maintain uniform feeding of sand, and Figure 1(b) shows the sand-filled gravel bed without any local depositions and bed form. The sidewalls of the flume at the test section were made of 3.5 m long transparent glasses to facilitate visual observation as shown in Figure 1(c). The gravel-bed surface profile is drawn from the bed surface fluctuations along the centreline of the flume. A Vernier point gauge was used to measure the gravel-bed surface fluctuations under clear-water flow conditions at 5 mm intervals. To obtain desirable flow conditions, the flow depth was monitored by an adjustable tailgate installed at the tail end of the flume. Three-point gauges with an accuracy of ± 0.1 mm were used to examine the uniform flow depth in the flume.

At the inlet, there existed a concrete stilling basin through which water entered into the flume. The stilling basin consisted of two steel perforated plates covering the full cross section for damping the flow turbulence and waves. The test section was located 8.8 m from the upstream end of the flume. After achieving the uniform flow conditions, the sediment was added into the flows at uniform rates as given in Table 1. At the beginning, the inter-gravel spaces from the flume bottom up to the mean bed level were filled very rapidly and the water surface level was found disturbed. The flow and sediment feeding were continued over the gravel–sand bed till the sand entrainment and deposition maintained a uniform sand bed level. The vertical distance between the average sand elevations to the gravel crest is referred to as z_s. The average thickness of the sand deposition was considered as the difference in elevation between the mean bed level ($z_1 = 0$) and average sand elevation (z_s). The present experimental work was carried out with four different sediment depositions as shown in Figure 2(a)–2(e). The

Figure 1 | Photographs of the experimental setup: (a) long section of a gravel bed, (b) long section of a sand-filled gravel bed and (c) side view of the sand-fill process.

Table 1 | Hydraulic conditions

$Q = 0.080$ m^3/s; $h = 0.164$ m; $S = 0.25\%$; $g_b = 1.77 \times 10^{-1}$ kg/ms

Flow conditions		U (m/s)	F	u_{*s} (m/s)	$u_{*\tau}$ (m/s)	Δz^+	z_0^+	κ
Unimodal gravel bed	Clear water flows (CW)	0.575	0.453	0.054	0.062	0.435	0.038	0.408
Bimodal gravel bed	$z_s = 1.63$ cm	0.541	0.426	0.054	0.06	0.425	0.040	0.39
	$z_s = 1.5$ cm	0.525	0.413	0.054	0.058	0.412	0.041	0.39
	$z_s = 1.0$ cm	0.522	0.411	0.054	0.056	0.375	0.043	0.38
	$z_s = 0.5$ cm	0.515	0.406	0.054	0.053	0.35	0.044	0.37

h, depth of flow; U, mean velocity; F, Froude number; g_b, sediment feed rate per unit width; u_{*s}, shear velocity determined from bed slope; $u_{*\tau}$, shear velocity evaluated from stress profile; κ, von Kármán coefficient; z_s, mean level of sand-filled gravel bed from the gravel crest; Δz^+, non-dimensional Nikuradse zero-plane displacement; z_0^+, non-dimensional depth of zero-velocity level.

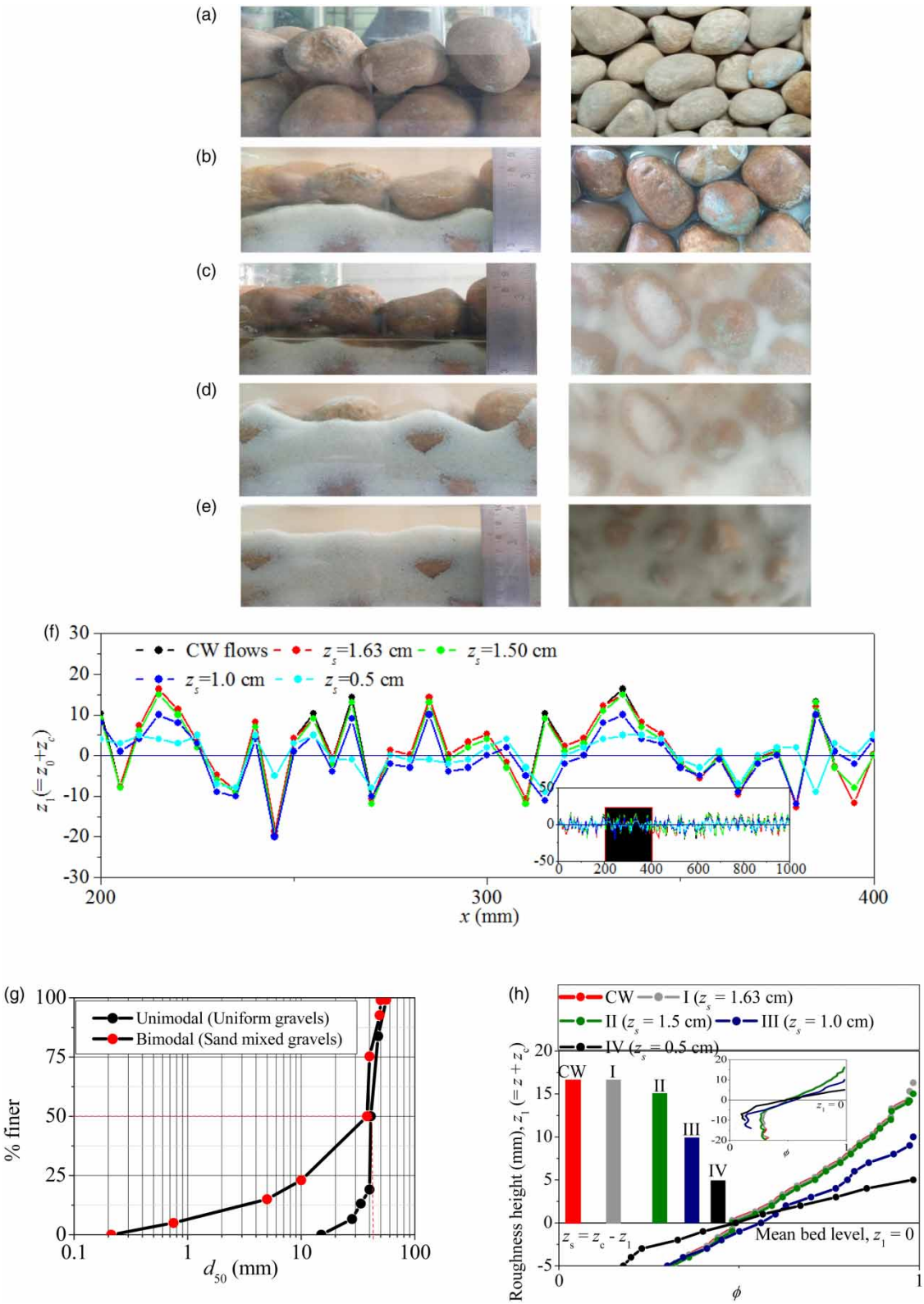

Figure 2 | Photographs of gradual sand-fill process (a) CW, (b) $z_s = 1.63$ cm, (c) $z_s = 1.5$ cm, (d) $z_s = 1$ cm, (e) $z_s = 0.5$ cm, (f) bed surface fluctuations for all, (g) grain size distributions of bed materials, and (h) sediment thickness measured from ϕ-distributions.

sediment was fed at a rate of 1.77×10^{-1} kg/ms to obtain four types of sand-infilled gravel beds. The average elevation of the sand-filled bed was measured at 5 mm intervals along the centreline of the flume by using a Vernier point gauge. The mean sand elevations relative to the gravel-bed crest are estimated as $z_s = 1.63$, 1.5, 1, and 0.5 cm by the Vernier point gauge. A line sketched through the mean values of the bed surface fluctuations corroborate the mean bed level ($z_1 = 0$), whereas the crest level (z_c) is characterised by the vertical distance from the mean bed level to the gravel crest as shown in Figure 2(f). The crest level of the gravel bed (z_c) was estimated to be 0.0163 m above the mean bed level. The average roughness height (k_s) of the gravel bed was evaluated from the standard deviation of the bed surface fluctuations and estimated to be 0.0093 m. The shear-particle Reynolds numbers $R_* = d_{50}u_*/\upsilon$ (u_* = shear velocity and υ = kinematic viscosity of fluid) were close to or greater than 70, indicating rough-turbulent flow conditions. The grain size distributions of the unimodal and bimodal beds are presented in Figure 2(g). The average thickness of the sediment depositions was also examined and estimated from the roughness geometry function (ϕ). The laboratory test for ϕ-distributions of the unimodal gravel bed and four cases of sand-filled gravel beds were carried out by the water displacement method (WDM) conducted in a glass container of size 30 cm × 30 cm × 30 cm. The test details are presented in another investigation by the authors on gravel-bed hydrodynamics (Dey & Das, 2012). The volume of added water in the container and the corresponding water level increment enable to plot the ϕ-distributions ($=V_f/V_0$, where V_f is volume liquid and V_0 is total volume). A 5-cm down-looking acoustic Doppler velocimeter (ADV), named *Vectrino*, manufactured by Nortek, was used to measure the instantaneous velocity components. The instrument functioned with an acoustic frequency of 10 MHz and a sampling rate of 100 Hz. The sampling volume was 6 mm diameter with 1–9.1 mm adjustable height. The instrument comprises one transmitting transducer and four receiving transducers. Addition of a fourth receiver improves turbulence measurements and provides redundancy. As the measuring location was 5 cm below the probe, there was no significant influence of the *Vectrino* probe on the measured data. The signal–noise ratio (SNR) was maintained above 15. Samplings were taken at different time instants to perform the uncertainty analysis for time-averaged velocities and the root mean square (RMS) of velocity fluctuations. The errors were within ±5 to ±8%, confirming the capability of the measurements by the Vectrino with 100 Hz frequency. The acoustic sensor incident and reflected pulses in some cases produced spikes in the Vectrino data and were filtered by acceleration threshold criteria (Goring & Nikora 2002). The velocity power spectra after filtration conform the Kolmogorov '–5/3 scaling-law' in the inertial sub-range for $f > 1$ Hz, corroborating the adequacy of the ADV measurements. The complete data filtration process is demonstrated in the authors' other experimental work (Dey & Das, 2012).

RESULTS AND DISCUSSION

Time-averaged flow characteristics

Figure 3(a)–3(c) present the normalised time-averaged streamwise velocity, RSS, and turbulence intensities over the immobile gravel bed under clear-water flow conditions and four cases of sand-filled gravel beds. The time-averaged streamwise velocity ($\bar{u}$) is normalised by the shear velocities u_* obtained from the RSS profile extrapolating them at the bed, whereas the ordinates of flow depth (z) are normalised by zero-plane displacement height (Δz). The data gathered from the experimental results show that the log-law that expresses the streamwise velocity distributions can be expressed as follows:

$$u^+ = 2.43 \ln\left[\frac{(z + \Delta z)/\Delta z}{(z_0/\Delta z)}\right] \tag{1}$$

where $u^+ = \bar{u}/u_*$, z_0 is the zero-velocity level, and Δz is the Nikuradse zero-plane displacement. To fit the data to the log-law given by Equation (1), the assessment of Δz, κ and z_0 were carried out by regression analysis of velocity data within the wall-shear layer ($z^+ < 0.1$, where $z^+ = z/h$). The value of log-law parameters in case of a gravel bed under clear-water conditions (without sediment depositions) are found as $\Delta z^+ = 0.375$, $\kappa = 0.408$, and $z_0^+ = 0.038$, whereas the traditional values of log-law parameters over a rough bed are $\Delta z^+ = 0.35$, $\kappa = 0.41$, and $z_0^+ = 0.033$ (Van Rijn, 1984). Conversely, in the case of the four sand-infilled gravel beds ($z_s = 1.63$, 1.5, 1.0, and 0.5 cm), the average values of the log-law parameter are estimated to be $\Delta z^+ = 0.34$, $\kappa = 0.38$, and $z_0^+ = 0.045$, respectively. The vertical distributions of time-averaged velocity over the gravel bed with sediment depositions ($z_s = 1.63$, 1.5, 1.0, and 0.5 cm) and under clear-water flow conditions are found well fitted to the logarithmic law of the wall above the crest level as shown in Figure 3(a). Importantly, the u^+-profiles deviate significantly at the gravel crest level and follow the polynomial below the crest level. Figure 3(a) shows the behaviour of u^+ with $(z + \Delta z)/\Delta z$ for the gravel bed under clear-water flow conditions and four sand-infilled gravel beds ($z_s = 1.63$, 1.5, 1.0, and 0.5 cm).

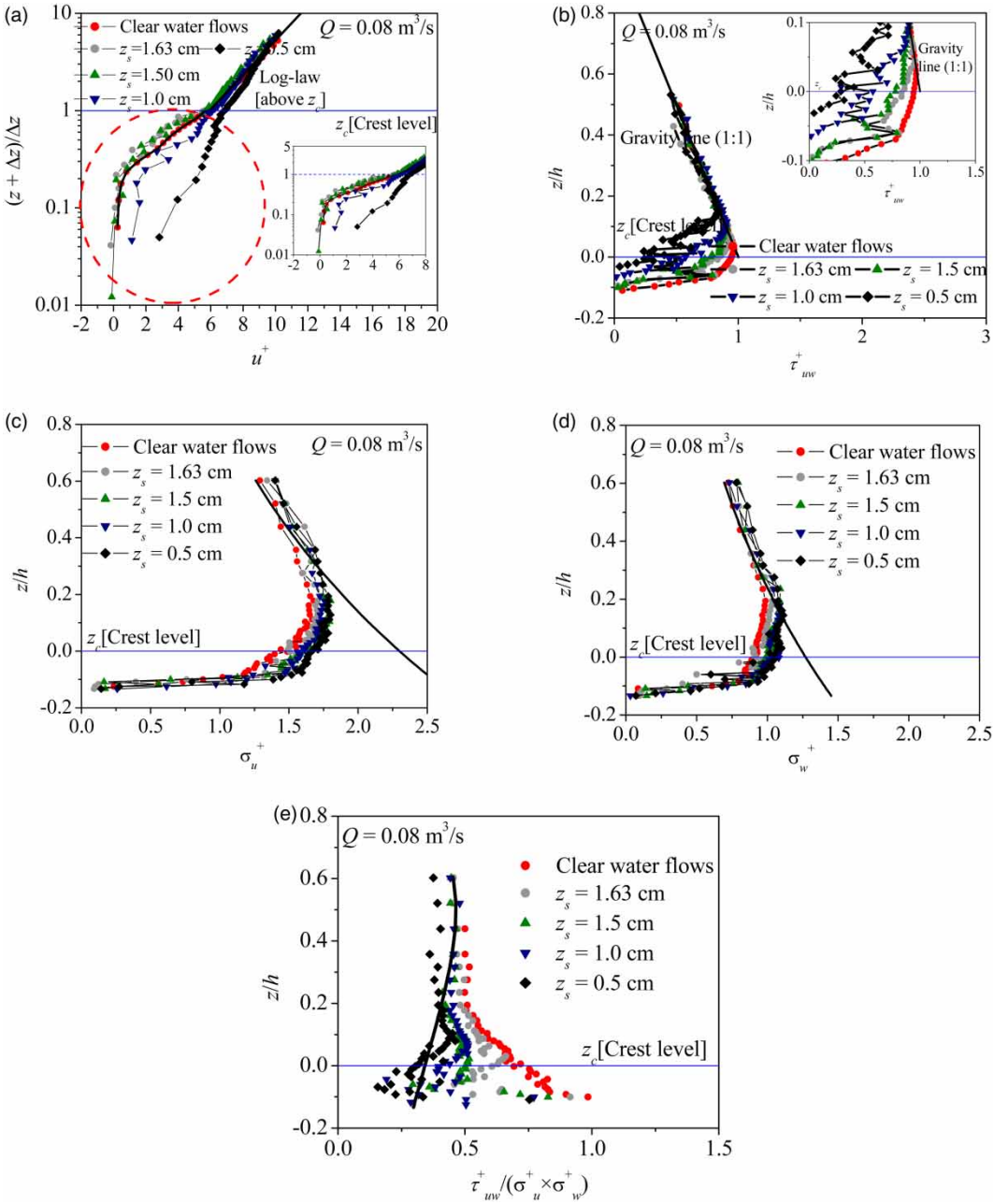

Figure 3 | Time-averaged flow characteristics: (a) streamwise velocity distributions, (b) Reynolds shear stresses, (c) streamwise turbulent intensities, (d) vertical turbulent intensities, and (e) ratio of Reynolds shear stresses to turbulent intensities.

Figure 3(b) presents the vertical distributions of the normalised RSS $\tau^+_{uw}(= -\overline{u'w'}/u_*^2)$ and the data plots within the wall-shear layer ($z^+ < 0.1$) in a larger scale. In the flow-layer $z^+ > 0.1$, the data plots for all the cases collapse on the so-called gravity line $\tau^+_{uw} = 1 - (z/h)$, for the free surface flows with a zero-pressure gradient. Importantly, the distributions of τ^+_{uw} for gravel-bed under clear-water flow conditions and sand-infilled gravel beds depict a strong departure from the linear law of $-\overline{u'w'}$. In the near-bed flow region ($z^+ < 0.1$), τ^+_{uw} for the sand-infilled beds diminish more in comparison with those on the gravel bed under clear-water flow conditions. The shear velocities u_* obtained from $-\overline{u'w'}$-distributions for all cases of sand-infilled beds are consistently less than those obtained from the gravel bed under clear-water conditions. The reduction in magnitude of u_* for sand-infilled beds is the result of the transfer of fluid turbulent stress to the bed particles to overcome the frictional resistance. Figure 3(b) shows that the τ^+_{uw}-profile attains maximum values at $z/h = 0.029$, 0.051, 0.85, and 0.10 in case of

$z_s = 1.63$, 1.5, 1.0, and 0.5 cm, respectively, and then decreases towards the lowest bed level. The gradual reductions of τ^+_{uw} resulted in massive damping of τ^+_{uw} below the crest. The normalised time-averaged streamwise and vertical turbulent intensities σ^+_u and σ^+_w are presented in Figure 3(c) and 3(d). The streamwise and vertical turbulent intensities are expressed as $\sigma_u = (\overline{u'u'})^{0.5}$ and $\sigma_w = (\overline{w'w'})^{0.5}$, respectively. Both the flow characteristics are normalised as $(\sigma^+_u, \sigma^+_w) = (\sigma_u, \sigma_w/u_*)$. The σ^+_u-profiles for gravel bed under clear-water flow conditions and sand-infilled gravel beds ($z_s = 1.63$, 1.5, 1.0, and 0.5 cm) show similar trends except over the bed crest level. Figure 3(c) shows that below the crest level σ^+_u increases with z/h and attains peak value at the vicinity of the crest level at $z/h = -0.01$ for the gravel bed under clear-water flow conditions and sand-infilled gravel beds $z/h = -0.002$, -0.002, -0.01, -0.02 for $z_s = 1.63$, 1.5, 1.0, and 0.5 cm.

Above the crest level, all the profiles experience slight reduction with further increase in z/h with a sequence of magnitude $\sigma^+_{u\,\mathrm{CW}} < \sigma^+_{u\,(zs=1.63)} < \sigma^+_{u\,(zs=1.5)} < \sigma^+_{u\,(zs=1.0)} < \sigma^+_{u\,(zs=0.5)}$. This depicts that the magnitude of σ^+_u is positively related with the thickness of sediment depositions on the gravel bed. Figure 3(d) shows the distributions of the normalised time-averaged vertical turbulent intensities, σ^+_w with z/h, and depicts similar trends with peak magnitude at the vicinity of the roughness crest level. Nezu & Nakagawa (1993) proposed an exponential law for the estimation of σ^+_u and σ^+_w as follows:

$$\sigma^+_u = D_u \exp(-c_u z/h) \tag{2}$$

$$\sigma^+_w = D_w \exp(-c_w z/h) \tag{3}$$

where $D_{u,w}$ and $c_{u,w}$ are the empirical parameters determined experimentally in a laboratory for open channel flow (Nezu & Nakagawa 1993). Figure 3(c) and 3(d) show that the data gathered in σ^+_u and σ^+_w are underestimated by the theoretical estimation and this is attributed to different experimental conditions. The drastic drop of σ^+_u and σ^+_w below the crest level are due to the reduction in temporal velocity fluctuations (u' and w'). Figure 3(e) shows the distributions of $\tau^+_{uw}/(\sigma^+_u \times \sigma^+_w)$ with z/h for a gravel bed under clear-water flow conditions and over a gravel bed with sediment depositions ($z_s = 1.63$, 1.5, 1.0 and 0.5 cm). The data plots above the roughness crest are well in agreement with Nezu & Nakagawa (1993) and it is apparent that the τ^+_{uw} is well in agreement in the central most region with the theoretical estimation, but below the gravel crest level the data points are largely scattered indicating higher flow heterogeneity in this zone.

TKE flux

The results of time-averaged flow characteristics in the previous section in some way enhance our understanding of the influence of bimodal deposits on the mean flow characteristics and turbulent stresses. This section elucidates the TKE fluxes to interpret the possible reason for the damping in the time-averaged RSS profiles at the vicinity of the crest level. Figure 4(a) and 4(b) show the vertical distributions of dimensionless streamwise and vertical TKE fluxes, $f^+_{ku} = f_{ku}/u^3_*$, where $f_{ku} = 0.5(\overline{u'u'u'} + \overline{u'v'v'} + \overline{u'w'w'})$, and $f^+_{ku} = f_{kw}/u^3_*$, where $f_{kw} = 0.5(\overline{u'u'w'} + \overline{v'v'w'} + \overline{w'w'w'})$. The profiles of f^+_{ku} and f^+_{ku} in the gravel bed under clear-water flow conditions are compared with those measured on the sand-infilled gravel-bed ($z_s = 1.63$, 1.5, 1.0, and 0.5 cm). In all the test beds, the f^+_{ku} starts with positive values below the crest level and increases gradually with the flow depth. The f^+_{ku} attains a peak value below the crest at $z^+ = -0.055$ in the case of the gravel bed under

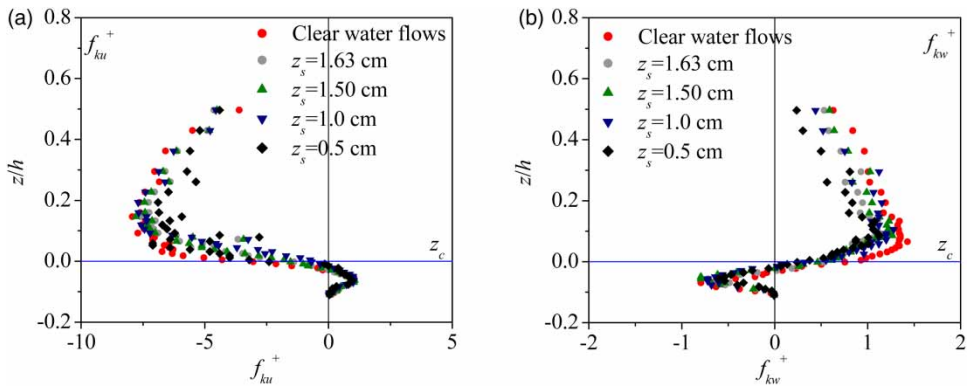

Figure 4 | Time-averaged TKE fluxes: (a) streamwise TKE fluxes and (b) vertical TKE fluxes.

clear-water flow conditions, whereas the f_{ku}^{+} in the sand-filled gravel bed reaches peak values relatively at higher locations at $z^{+} = -0.069$, -0.055, -0.048, -0.049 for $z_s = 1.63$, 1.5, 1.0, and 0.5 cm, respectively. In a similar vein, the f_{kw}^{+} profiles on the gravel bed under clear-water conditions $z^{+} = -0.069$ and sand-filled gravel beds start with small negative values below the crest level as shown in Figure 4(b) and reach negative peak values at $z^{+} = -0.028$, -0.035, -0.028, and -0.028 for $z_s =$ 1.63, 1.5, 1.0, and 0.5 cm, respectively. The magnitudes of f_{ku}^{+} gradually decrease attaining negative peaks towards the upper boundary of the roughness layers. The positive and negative f_{ku}^{+} indicate streamwise and upstream transport of the TKE flux, respectively, whereas the positive and negative f_{ku}^{+} values corroborate upward and downward transport, respectively (Dey & Raikar, 2007). Therefore, it is interpreted that the opposite nature of f_{ku}^{+} and f_{ku}^{+} in the interfacial sublayer results in slowing down the time-averaged Reynolds shear stresses at the vicinity of the sand-infilled gravel-bed surface.

Turbulent bursting events

Turbulent bursting events are analysed by plotting the temporal streamwise and vertical velocity fluctuations (u' and w') on a $u'w'$-plane (Lu & Willmarth, 1973). The bursting events are characterised by four quadrants: (1) outward interactions, Q1 (u', $w' > 0$), (2) ejections, Q2 ($u' < 0$, $w' > 0$), (3) inward interactions, Q3 (u', $w' < 0$), and (4) sweeps, Q4 ($u' > 0$, $w' < 0$). The dominance of an event to the RSS is characterised by the contributions of u' and w' from each quadrant (Nezu & Nakagawa 1993). The quadrant plot of temporal velocity fluctuations, u' and w' measured at crest level is presented in Figure 5(a) and 5(b). Both the temporal velocity fluctuation components u' and w' are normalised by multiplying $(u_*)^{-1}$. It is apparent that in the case of the gravel bed under clear-water conditions, the contributions of ejection events ($u' < 0$, $w' > 0$) and sweep events ($u' > 0$, $w' < 0$) are evaluated as 86 and 56%, respectively. Conversely, the contributions of ejection events and sweep events in the case of the sand-infilled gravel bed are estimated as 80 and 60%, respectively, which reveals that the sweep events are dominant in sediment-deposited gravel-bed streams.

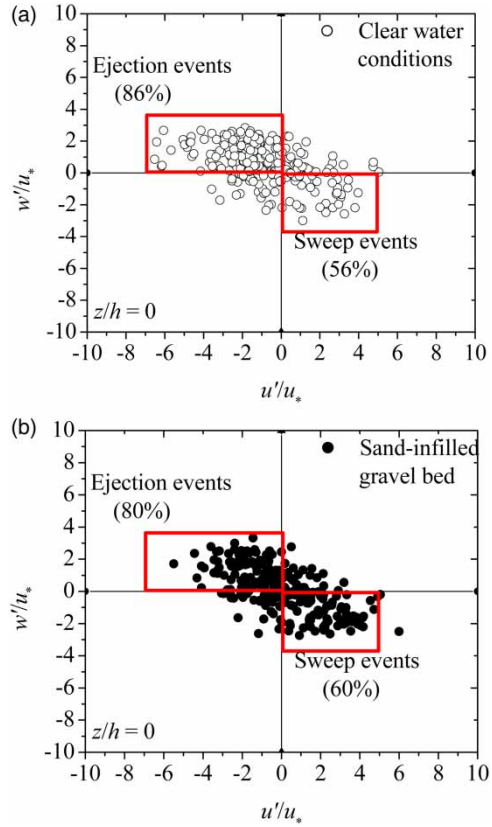

Figure 5 | Quadrant plot of temporal velocity fluctuations, u' and w' measured at crest level: (a) clear-water conditions and (b) sand-infilled gravel bed.

Moreover, the quadrant analysis of conditional Reynolds shear stresses (CRSS) is presented in Figure 6(a)–6(e). It is apparent from the data plots of CRSS that at the vicinity of the crest level ($z/h = 0$) for all the cases, the contributions of ejection events (Q2: $u' < 0$, $w' > 0$) to the RSS production is larger than the contributions from sweep events (Q4: $u' > 0$, $w' < 0$) and this trend continues up to the free surfaces, whereas the contributions from outward interaction (Q1: $u' > 0$, $w' > 0$) and inward interaction (Q3: $u' < 0$, $w' < 0$) events are insignificant as commonly observed in rough bed flows (Pokrajac & Lemos 2015; Padhi *et al.* 2020). It is pertinent to mention that the ejection event develops low-speed liquid away from the boundary and the sweep events mainly associated with high-speed liquid towards the boundary. Similarly, the outward interactions and inward interactions refer to weak outward interactions of liquid away from the boundary and weak inward interactions of liquid towards the boundary, respectively. Importantly, below the crest level and at the vicinity of the deposited finer sediment, it is apparent that the contribution from the sweep events increases and is found higher in all the sand-filled gravel beds than those in the gravel bed under clear-water flow conditions. The sequences of bursting events in the case of the

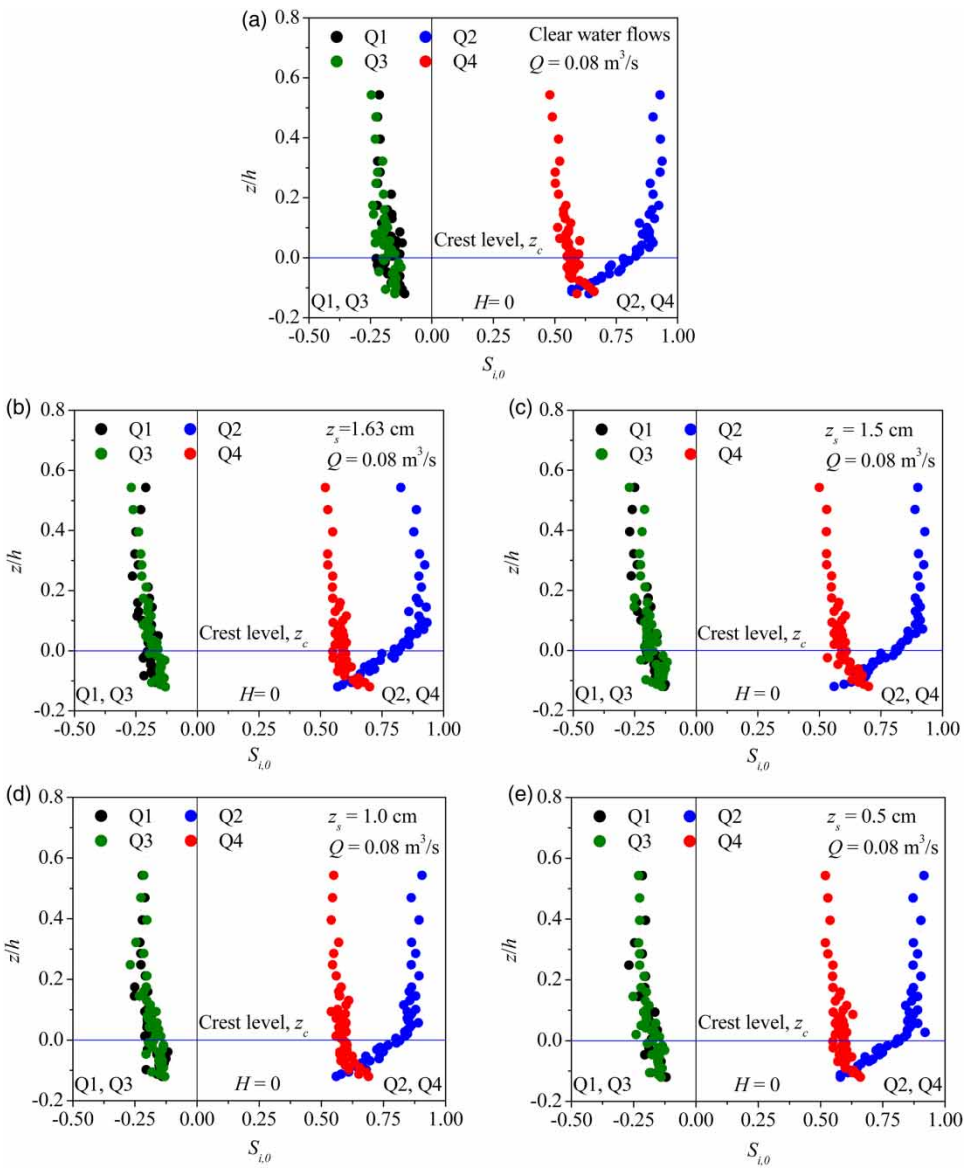

Figure 6 | Vertical distributions of CRSS to total shear stress: (a) clear-water flows, (b) $z_s = 1.63$ cm, (c) $z_s = 1.50$ cm, (d) $z_s = 1.0$ cm, and (e) $z_s = 0.5$ cm.

gravel bed under clear-water conditions and the sand-filled gravel beds are presented in Figure 7(a)–7(c). The analysis is performed at three elevations (below the crest, at the crest, and above the crest level). At the gravel-bed crest level under clear-water conditions, the contributions from ejection and sweep events are approximately 86 and 56%, respectively. The contributions from Q1 and Q3 events are approximately 13 and 14%, respectively. At the same location (crest level) in case of $z_s = 1.63$ cm, the contributions of ejection and sweep events are 80 and 60%, whereas Q1 and Q3 events are approximately 15 and 11%, respectively. This depicts that the sediment entrainment and deposition enhance the contributions of turbulent sweep events. Moreover, the contributions of sweep events increase below the crest level and decrease above the crest level in all the cases of gravel beds with sediment depositions.

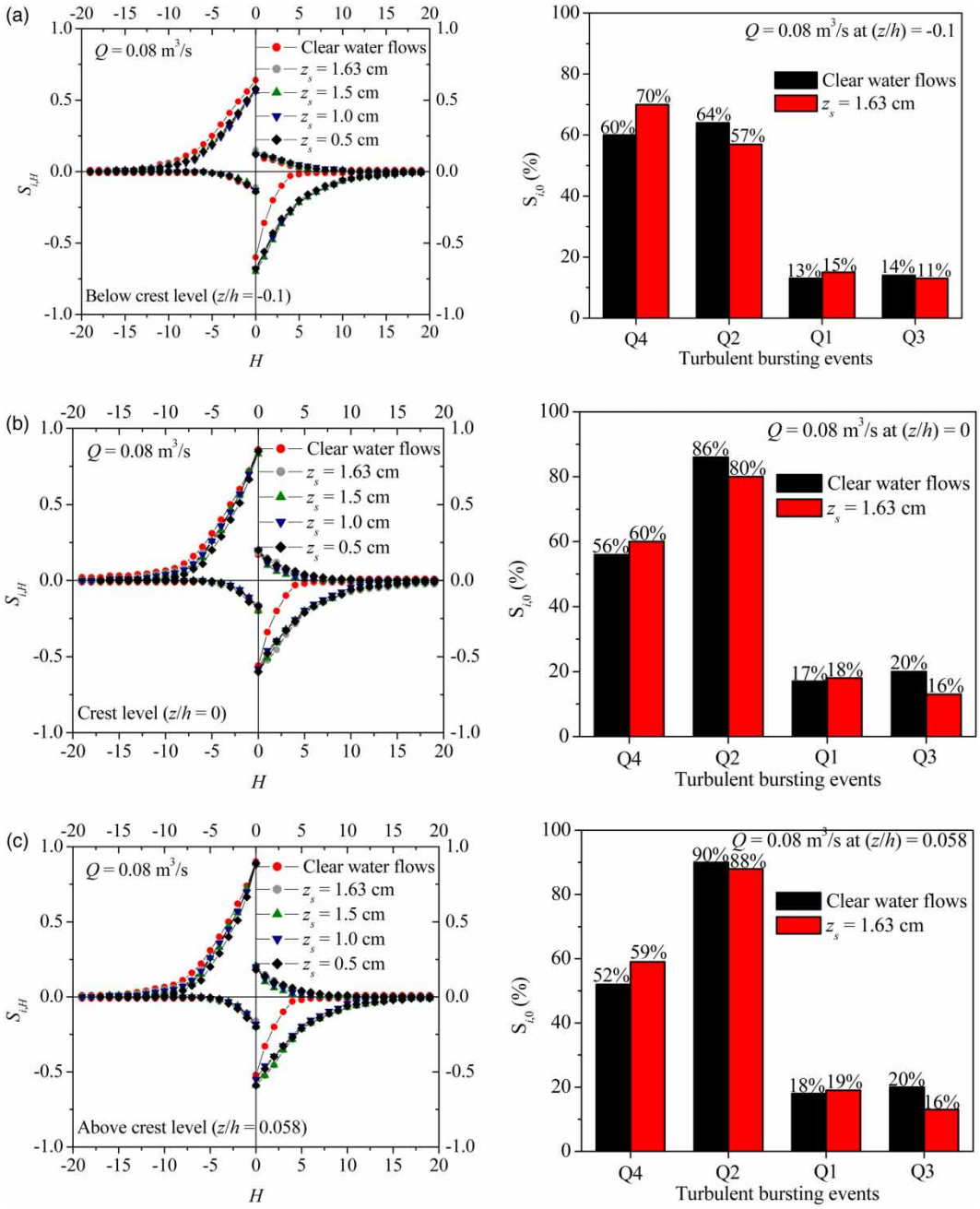

Figure 7 | Quadrant and bar chart analysis for $Q = 0.08$ m^3/s: (a) mean bed level, (b) crest level, and (c) away bed region.

CONCLUSIONS

Sediment depositions in an immobile gravel-bed stream and their influence on the near-bed turbulent flow characteristics are studied experimentally. Mean flow characteristics over sand-filled gravel beds at four different elevations are analysed. The results are compared with those over the gravel bed under clear-water flow conditions. The important conclusions are enumerated as follows:

1. The time-averaged streamwise velocity profiles are found well in agreement with the logarithmic law of the wall above the stream bed crest level. The log-law parameters are characterised by increasing the zero-plane displacement height and zero-velocity level owing to the increasing thickness of sand depositions in gravel-bed streams in comparison with the gravel-bed flows under clear-water flow conditions.
2. The time-averaged RSS distributions in the sand-filled gravel beds experienced larger damping in the near-bed flow region in comparison with those in the gravel bed under clear-water flow conditions.
3. In the near-bed flow zone, flow over the bimodal beds is associated with a positive streamwise and a negative vertical TKE flux, respectively, directing towards the flow and downward.
4. Conditional statistics of RSS showed that sweep events are the prevailing mechanism towards flow over a bimodal bed.

DATA AVAILABILITY STATEMENT

Data cannot be made publicly available; readers should contact the corresponding author for details.

CONFLICT OF INTEREST

The authors declare there is no conflict.

REFERENCES

Almedeij, J. H. & Diplas, P. 2003 Bedload transport in gravel-bed streams with unimodal sediment. *J. Hydraul. Eng.* **129** (11), 896–904.

Bathurst, J. C. 1987 Critical conditions for bed material movement in steep, boulder-bed streams. *Int. Assoc. Hydro. Sci. Publ.* **165**, 309–318.

Best, J. 2005 The fluid dynamics of river dunes: A review and some future research directions. *J. Geophys. Res.* **110**, F04S02.

Cellino, M. & Lemmin, U. 2004 Influence of coherent flow structures on the dynamics of suspended sediment transport in open-channel flow. *J. Hydraul. Eng.* **130** (11), 1077–1088.

Dey, S. & Das, R. 2012 Gravel-bed hydrodynamics: Double-averaging approach. *J. Hydraul. Eng.* **138** (8), 707–725.

Dey, S. & Raikar, R. V. 2007 Characteristics of loose rough boundary streams at near threshold. *J. Hydraul. Eng.* **133** (3), 288–304.

Dey, S., Sarkar, S., Bose, S. K., Tait, S. & Castro-Orgaz, O. 2011 Wall-wake flows downstream of a sphere placed on a plane rough wall. *J. Hydraul. Eng.* **137** (10), 1173–1189.

Dietrich, W. E., Whiting, P. J., 1989 Boundary shear stress and sediment transport in river meanders of sand and gravel. In: *River Meandering, American Geophysical Union Water Resources Monograph*, Vol. 12 (Ikeda, S. & Parker, G., eds). American Geophysical Union, Washington, DC.

Drake, T. G., Shreve, R. L., Dietrich, W. E., Whiting, P. J. & Leopold, L. B. 1988 Bedload transport of fine gravel observed by motion picture photography. *J. Fluid Mech.* **192**, 193–217.

Ferguson, R. I., Prestegaard, K. L. & Ashworth, P. J. 1989 Influence of sand on hydraulics and gravel transport in a braided gravel bed river. *Water Resour. Res.* **25**, 635–643.

Gaudio, R., Miglio, A. & Calomino, F. 2011 Friction factor and von Karman's (in open channels with bed-load. *J. Hydraul. Res.* **49**, 245–253.

Goring, D. G. & Nikora, V. I. 2002 Despiking acoustic Doppler velocimeter data. *J. Hydraul. Eng.* **128** (1), 117–126.

Grams, P. E. & Wilcock, P. R. 2007 Equilibrium entrainment of fine sediment over a coarse immobile bed. *Water Resour. Res.* **43**, W10420.

Gyr, A. & Schmid, A. 1997 Turbulent flows over smooth erodible sand beds in flumes. *J. Hydraul. Res.* **35** (4), 525–544.

Heathershaw, A. D. & Thorne, P. D. 1985 Sea-bed noises reveal role of turbulent bursting phenomenon in sediment transport by tidal currents. *Nature.* **316**, 339–342.

Iseya, F. & Ikeda, H. 1987 Pulsations in bedload transport rates induced by a longitudinal sediment sorting: A flume study using sand and gravel mixtures. . *Geogr. Ann., Series A, Phys. Geogr.* **69**, 15–27.

Lu, S. S. & Willmarth, W. W. 1973 Measurements of the structures of the Reynolds stress in a turbulent boundary layer. *J. Fluid Mech.* **60**, 481–511.

Nezu, I. & Nakagawa, H. 1993 *Turbulence in Open-Channel Flows*. Balkema, Rotterdam, Netherlands.

Padhi, E., Dey, S., Desai, V. R., Penna, N. & Gaudio, R. 2020 Water-worked gravel bed: State-of-the-art review. *Water* **11** (4), 694.

Pokrajac, D. & Lemos, M. J. S. 2015 Spatial averaging over a variable volume and its application to boundary-layer flows over permeable walls. *J. Hydraul. Eng.* **141** (4), 04014087.

Robert, A., Roy, A. G. & Serres, B. D. 1992 Changes in velocity profiles at roughness transitions in coarse grained channels. *Sedimentology* **39**, 725–735.

Sambrook Smith, G. H. & Ferguson, R. I. 1995 The gravel-sand transition along river channels. *J. Sediment. Res. A* **65**, 423–430.

Sambrook Smith, G. H. & Ferguson, R. I. 1996 The gravel-sand transition: Flume study of channel response to reduced slope. *Geomorphology* **16**, 147–159.

Sambrook Smith, G. H. & Nicholas, A. P. 2005 Effect on flow structure of sand deposition on a gravel bed: Results from a two-dimensional flume experiment. *Water Resour. Res.* **41**, W10405.

Sharma, A. 2021 Velocity distribution and the moments of turbulent flow over a sand-gravel mixture bed. *Water Resour.* **48** (6), 960–966.

Shih, W., Diplas, P., Celik, A. O. & Dancey, C. 2017 Accounting for the role of turbulent flow on particle dislodgement via a coupled quadrant analysis of velocity and pressure sequences. *Adv. Water Resour.* **101**, 37–48.

Thorne, P. D., Williams, J. J. & Heathershaw, A. D. 1989 In situ acoustic measurements of marine gravel threshold and transport. *Sedimentology* **36**, 61–74.

Van Rijn, L. C. 1984 Sediment transport. Part I: Bed-load transport. *J. Hydraul. Eng.* **110** (10), 1431–1456.

Wallace, J. M. 2016 Quadrant analysis in turbulence research: History and evolution. *Annu. Rev. Fluid Mech.* **48**, 131–158.

Wilcock, A. 1993 A theory of the human need for occupation. *J. Occup. Sci.* **1** (1), 17–24.

Wilcock, P. R. & Kenworthy, S. T. 2002 A two fraction model for the transport of sand/gravel mixtures. *Water Resour. Res.* **38** (10), 12–11.

Williams, J. J., Bell, P. S. & Thorne, P. D. 2003 Field measurements of flow fields and sediment transport above mobile bed forms. *J. Geophys. Res.* **108** (C4), 3109.

Wren, D. G., Langendoen, E. J. & Kuhnle, R. A. 2011 Effect of sand addition on turbulent flow over an immobile gravel bed. *J. Geophys. Res.* **116**, F01018.

Yuan, Y., Wei, H., Zhao, L. & Cao, Y. 2009 Implications of intermittent turbulent bursts for sediment resuspension in a coastal bottom boundary layer: A field study in the western Yellow Sea, China. *Mar. Geol.* **263** (1–4), 87–96.

First received 19 October 2023; accepted in revised form 2 February 2024. Available online 21 February 2024